Nanoparticles Self-Assembly

DOI: 10.1002/anie.201204583

PbS–Organic Mesocrystals: The Relationship between Nanocrystal Orientation and Superlattice Array**

Paul Simon, Elena Rosseeva, Igor A. Baburin, Lydia Liebscher, Stephen G. Hickey, Raul Cardoso-Gil, Alexander Eychmüller, Rüdiger Kniep, and Wilder Carrillo-Cabrera*

The ability to prepare nanostructured and/or nanocomposite materials on a large scale by simple and controllable routes still remains a challenge in chemistry and material science. By employing well-established synthetic strategies, nanoparticles with different sizes, shapes and compositions can be readily produced. The high tendency for self-aggregation and self-organization of these nanosized building blocks, which are surface-stabilized by organic molecules, into superstructures has been used to create 2D and 3D assemblies.[1–9] In the last decade, a series of 3D colloidal superlattices composed of different nanoparticles (Ag, Au, PbS, PbSe, CeO_2, FePt, $CoPt_3$, Fe_3O_4, PbSe/Au, Fe_2O_3/PbSe, PbSe/Pd, CdSe/PbSe, etc.) has been reported.[10–20] Particularly, PbS–organic nanoparticles of different shapes (including cubes, octahedra, truncated octahedra, rhombicuboctahedra, etc.) can be easily synthesized on a large scale, and attracted much attention[15,16,21,22] because of a variety of possible applications.[23–27] Therefore, this kind of system provides a chance to study diverse packing arrangements (e.g., *fcc*, *bcc*, etc.) and specific orientational ordering of nanoparticles.[11,13,15,16,28,29]

Experimental observations[16,29–34] suggest that nanoparticles within a colloidal crystal tend to arrange in such a way that the optimal packing efficiency is achieved (principle of maximum space filling[35]). In a relatively common case of truncated octahedrally shaped nanoparticles, the available experimental data[4,5,16,29–33,36] allow to rationalize the formation of a particular type of the superlattice array (depending on the degree of coverage of nanocrystals by organic molecules) by considering four phenomenological models:

A) Rigid, anisotropically shaped space-filling nanoparticles (inorganic part) without or with a tiny shell of organic molecules;
B) Hard spheres with a comparatively large anisotropic core (inorganic part) covered by a relatively thin shell of organic molecules;
C) Hard spheres with a comparatively small anisotropic core (inorganic part) and a thick shell of organic molecules;
D) Soft and easily deformable spheres with a small anisotropic core (inorganic part) and an even thicker shell of organic molecules.

For each case (A–D) the type of superlattice packing (translational order[37]) and orientational ordering of nanoparticles within the superlattice array is significantly different. In the simplest case (A), the more or less pure, inorganic, truncated octahedrally shaped nanoparticles assemble into a *bcc* superlattice[33] with 100 % packing efficiency and strong orientational relationship (crystallographic directions of nanocrystals are coaxial with those of the superlattice).[35,37] In case of models B and C, by increasing the degree of coverage of anisotropic (inorganic) nanoparticles by organic molecules, their faces are continuously smoothed, thereby introducing a certain orientational mismatch of the nanoparticles within the superlattice array.[16,29–31] Moreover, in both cases (B and C), nanoparticles self-assemble into an *fcc* packing.[38,39] Although the type of superlattice is kept (*fcc*), the extent of the orientational ordering of the nanoparticles decreases from B to C, such that the orientational ordering of the nanocrystals almost completely disappears in the latter case. In the case of model D, quasispherical nanoparticles with a thick shell of organic molecules (easily deformable spheres) tend to be assembled with the minimal overlap in order to avoid repulsive interactions as much as possible. If equal spheres (in this case monodisperse nanoparticles) have to be put together with the minimal possible overlap, this situation corresponds to the most economical covering of space by spheres (so-called "thinnest covering" in mathematics[40,41]), which is realised by the *bcc* arrangement.[32,36] Because of the thick organic shell, the orientational ordering of nanocrystals within this type of superlattice is low.

In the present contribution, we report on a comprehensive study of structural ordering within the 3D PbS–organic colloidal superlattice, and show an overall structure closely related to model B. Besides the type of the superlattice, we particularly focus on the orientational relations between nanocrystals, thus allowing us, for the first time, to develop the atomistic models that describe the structure of the colloidal superlattice in reasonable agreement with experimental data.

[*] Dr. P. Simon, Dr. E. Rosseeva, Dr. R. Cardoso-Gil, Prof. Dr. R. Kniep, Dr. W. Carrillo-Cabrera
Max Planck Institute for Chemical Physics of Solids
Nöthnitzer Straße 40, 01187, Dresden (Germany)
E-mail: Paul.Simon@cpfs.mpg.de
Dr. I. A. Baburin, M. Sc. L. Liebscher, Dr. S. G. Hickey, Prof. Dr. A. Eychmüller
Department of Physical Chemistry/Electrochemistry
TU Dresden
Bergstr. 66b, 01062, Dresden (Germany)

[**] We would like to thank Prof. Dr. Hannes Lichte for the possibility to perform TEM measurements at the Triebenberg Laboratory (TU Dresden) and Jana Buder for the ultramicrotomic preparation of thin cuts of mesocrystals. L.L. thanks the research training group "Nano- and Biotechnologies for Packaging of Electronic Systems" for a scholarship.

Supporting information for this article is available on the WWW under http://dx.doi.org/10.1002/anie.201204583.

The PbS–organic nanoparticles and the colloidal superlattices have been prepared as described by Nagel et al.[11] The PbS nanocrystals used for the formation of the superlattice were stabilized by a mixture of oleic acid (OA) and trioctylphosphine (TOP). The morphology of the as-grown aggregates was characterized by SEM (Figure 1 a and b). The

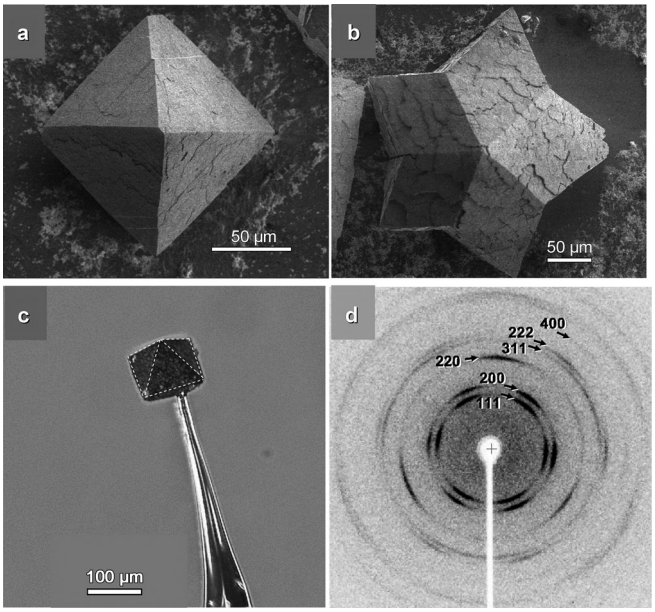

Figure 1. SEM images of PbS–organic colloidal crystals with a) octahedral and b) five-armed star morphologies. c) Light-microscope image of an octahedrally shaped specimen fixed on a glass string, and d) the corresponding X-ray diffraction pattern (Mo Kα radiation) along $[111]_{SL}$.

samples consist of regular octahedra (Figure 1 a) as well as various twinned and even five-armed (so-called "*stella quinquangula*") morphologies (Figure 1 b). To demonstrate that the inner structure of the aggregates is homogeneous, single specimens were polished and found to be free of internal cracks or grain boundaries on the micrometer level (see Figure S1 in the Supporting Information).

To obtain a first overall impression of structural ordering within the volume of the complete colloidal nanocrystal assembly, an octahedral specimen (Figure 1 c) was chosen for X-ray diffraction investigations. The Bragg part of the diffraction pattern (detected along [111] of the octahedrally shaped crystal; Figure 1 d) is characteristic for a texture-dominated material with particular ordering effects. The most interesting observation is the presence of sets of $(111)_{PbS}$ and $(200)_{PbS}$ reflections (the subscript PbS refers to the galena crystal structure), which should be absent in the diffraction pattern of a PbS single crystal detected along $[111]_{PbS}$. The angular width of the $(111)_{PbS}$, $(200)_{PbS}$, and $(220)_{PbS}$ reflections is approximately 15–20°. As a first approximation, the textured X-ray pattern can be interpreted as a superposition of diffraction patterns of PbS particles with preferred orientations nearly along $[111]_{PbS}$ and nearly along $[110]_{PbS}$, the $[110]_{PbS}$ species being rotated by 120° with respect to each other (a more detailed discussion is given below). The apparent differences in the intensities of the $(220)_{PbS}$ reflections (three weak and three strong) are a result of strong and direction-related absorption effects of the octahedrally shaped crystal.

The inner structure of the PbS colloidal nanocrystal assembly was further investigated by means of TEM images on focused ion beam (FIB) cuts (Figure S2, c and d). By using the FIB technique, artefacts, which might be caused by mechanical stress during preparation (e.g., as can be expected for conventional diamond cuts) or by swelling (as a result of the use of epoxy resin as embedding material) can be avoided. TEM investigations on FIB cuts were performed in the middle-resolution regime (magnification of about 160.000x). As a result, three different orientations of the superlattice (SL; denoted as $[100]_{SL}$, $[110]_{SL}$, and $[111]_{SL}$; see Figure 2 a, c,

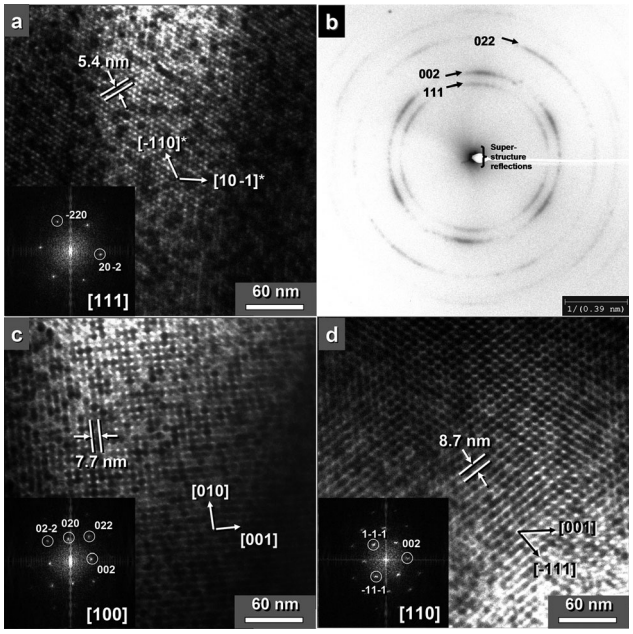

Figure 2. TEM images of FIB cuts with corresponding FFT insets, characterizing the arrangement of nanoparticles viewed along $[111]_{SL}$ (a), $[100]_{SL}$ (c), and $[110]_{SL}$ (d). b) Electron diffraction pattern from area (a). For further details see text.

and d) were identified to be consistent with a face-centered cubic (*fcc*) arrangement. The superlattice orientations were determined by using fast Fourier transforms (FFTs) of the direct images (see insets in Figure 2 a, c, and d). By combining the three different zones, the unit-cell parameter of the superlattice was found to be $a_{SL} = 15.4$ nm, which is in good agreement with the expected value for an *fcc* arrangement of nanoparticles with approximately 5.5 nm-sized PbS cores stabilized by oleic acid molecules of around 1.8 nm in length.[30] The $[111]_{SL}$ zone exclusively consists of a set of $(220)_{SL}$ reflections, exhibiting hexagonal symmetry and a lattice spacing of $d_{220} \approx 5.4$ nm (inset of Figure 2 a). The electron diffraction (ED) pattern obtained from the same area along $[111]_{SL}$ in the wide-angle region is similar to the XRD pattern obtained along $[111]_{SL}$ (Figure 2 b). In addition, the hexagonal shape of the central spot in the ED pattern (Figure 2 b) can be

interpreted as a blurred image (because of the high background of the primary beam) of the small-angle diffraction pattern, thus indicating the closed-packed structural motif of the nanoparticles along $[111]_{SL}$.

In order to reveal the shape of the individual nanoparticles, high-resolution TEM (HRTEM) was applied. For this purpose, we used thin cuts of samples prepared with a diamond knife (Figure S3 a–c). To observe individual nanoparticles, the colloidal crystal was soaked and partially swollen by penetration of the epoxide monomer, resulting in a diluted state, before hardening of the embedding material. Within the FIB cuts, the individual nanoparticles always overlap in viewing direction because of the closed-packed arrangement. By combining the two different projections (along $[100]_{PbS}$ and $[1-10]_{PbS}$; see Figure 3 a and e and

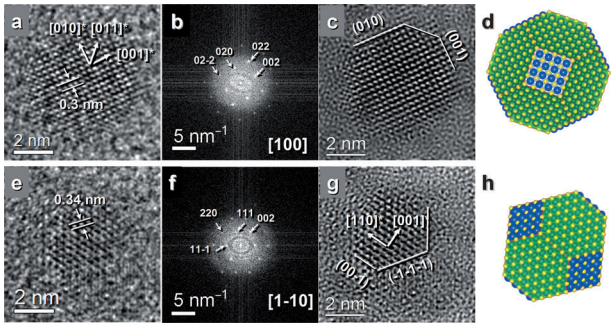

Figure 3. HRTEM images of nanoparticles viewed along $[100]_{PbS}$ (a) and $[1\text{-}10]_{PbS}$ (e); (b, f) corresponding FFTs; (c, g) filtered representations; (d, h) projections of simulated, truncated octahedrally shaped nanoparticles.

their filtered representations Figure 3 c and g), it becomes clear that the habit of a single particle ($\approx$5.5 nm in diameter) can be closely approximated by a truncated octahedron (Figure 3 d and h). The reflections in the corresponding FFTs (Figure 3 b and f) were indexed based on the galena crystal structure ($Fm\bar{3}m$, $a = 5.936$ Å[42]).

To further characterize the overall structure and orientational order of the nanoparticles within the colloidal superlattice, the dark-field (DF) TEM technique was applied. The DFTEM image was recorded using a small objective aperture, which was set on part of the diffractogram that exclusively contained one of the $(200)_{PbS}$ reflection arcs of PbS (Figure 4). The bright spots in the DFTEM image correspond to the nanoparticles with the same crystallographic orientation. They do not show any long-range translational order,[37] but rather short-range order could be evidenced. The superposition of the ideal models II and III is giving the domain structure of the real crystal. The simple packing order of the nanoparticles gives rise to a long-range order, as evidenced by appearance of Bragg reflections in the Fourier transform of the DFTEM image (not shown). However, if we also take the orientation order of the faceted nanoparticles into account, only short-range order can be detected.

In addition, some of the nanoparticles (the orientations of which do not fit to the selected Bragg condition) exhibit the

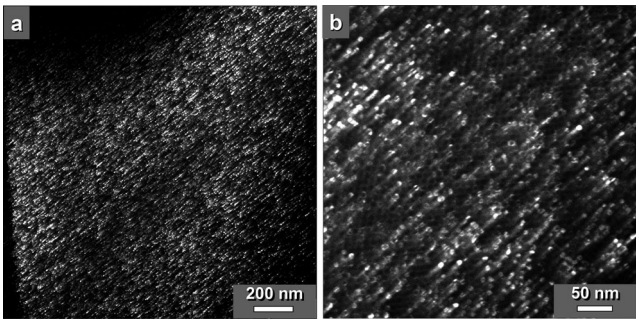

Figure 4. Dark-field TEM images of FIB cuts oriented along $[110]_{SL}$ and obtained by using a small objective aperture positioned on one of the $(200)_{PbS}$ reflection arcs. For further details see text.

so-called "ring contrast" with a bright ring at their edges, attributed to diffuse scattering from these particles.[6]

Electron holography on FIB cuts was applied to visualize the topography of the superlattice. Although electron holography is a powerful tool to image nanosized electrical and magnetic fields,[43] this study did not support the predicted existence of intrinsic electric dipole fields around the PbS nanoparticles[44] (Figure S4).

The PbS–organic colloidal superlattice reported here is different from all the previously structurally characterized systems of similar type.[29,30,32] In our system, the truncated octahedrally shaped PbS nanocrystals stabilized by organic molecules assemble into an *fcc* superlattice with long-range "translational" order, while still maintaining their preferable crystallographic orientation limited to shorter ranges. This situation reminds of a special type of colloidal crystals, which are classified as "mesocrystals" and represent superstructures of nanoparticles with certain mutual orientation relations.[45,46]

In order to get a better understanding of the specific structuring scenarios of the colloidal superlattice, we propose a hierarchy of models that simulate different kinds of orientational ordering of the nanoparticles within the *fcc* supperlattice of the mesocrystal. In order to build the most suitable model that characterizes the overall structure of the mesocrystal, a "multidomain" structure of the material is assumed, which is consistent with the results of the DFTEM investigations. Following this approach, three "simple" models were developed, approximating the structure of the domains (Figure 5). In the most simple case (model I, Figure 5 b), truncated octahedrally shaped PbS nanoparticles were arranged at the nodes of the *fcc* superlattice ($a_{SL} =$ 15.4 nm), thus keeping their crystallographic directions coaxial with those of the *fcc* superlattice (in this case, the parent symmetry of the galena crystal structure ($Fm\bar{3}m$) is kept). Nonetheless, the wide-angle region in the simulated electron diffraction pattern of the nanoparticles assembly (Figure 5 b) is significantly different from the experimental pattern that is recorded along the same direction ($[111]_{SL}$; see Figures 1 d and 2 a and b). This discrepancy was addressed by introducing two additional models in which the nanoparticles within the *fcc* superlattice were successively rotated in order to achieve the orientational relation $[111]_{SL} \parallel [110]_{PbS}$: first,

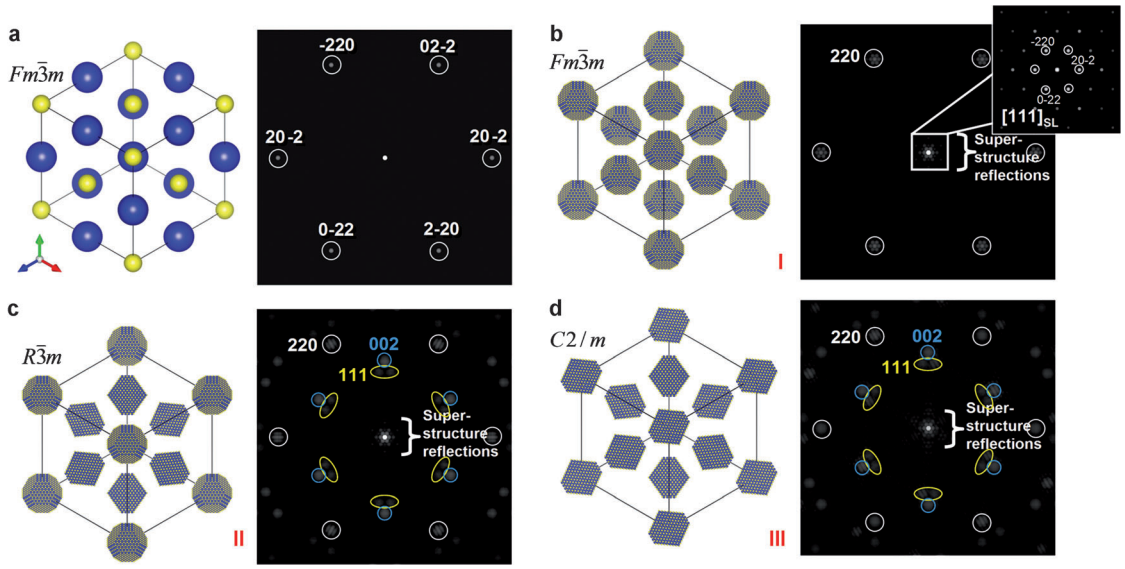

Figure 5. a) [111] Projection of the galena (PbS) crystal structure with corresponding simulated SAED pattern. $[111]_{SL}$ Projections of simulated PbS–organic colloidal crystals (models I (b), II (c), and III (d)) with corresponding simulated ED patterns, illustrating orientational relationships between the superstructure and the PbS (galena) nanocrystal reflections. The sets of equidistant (220), (002), and (111) PbS Bragg reflections are marked with white, blue, and yellow circles, respectively. In model I (b), truncated octahedrally shaped PbS nanoparticles are placed at the nodes of the fcc superlattice where the $[111]_{PbS}$ orientations of the nanoparticles are parallel with the $[111]_{SL}$ superlattice orientation. In model II (c), along $[111]_{SL}$ of superlattice, nanoparticles at the centers of fcc unit-cell faces have a $[110]_{PbS}$ orientation, while at the vertices $[111]_{PbS}$. Finally, in model III (d), all nanoparticles show the $[110]_{PbS}$ orientation parallel to the $[111]_{SL}$ zone of the superlattice. Nanoparticle habits and orientations are taken from Figure 3.

only at the centers of unit-cell faces (model II, Figure 5c), and afterwards also at the vertices (model III, Figure 5d). The space-group symmetries of the colloidal nanocrystal superlattices for models II and III are $R\bar{3}m$ and $C2/m$, respectively. The simulated ED patterns along $[111]_{SL}$ for these models (Figure 5c and d) are already closely related to the experimental ED pattern over the whole angle range (see Figure 2a and b). These results allow us to assume that the experimental electron diffraction pattern can be interpreted as a superposition of ED patterns (Figure 6) generated from the proposed structural models (especially models II and III), which closely approximate the structure of single domains within the multidomain structure of the PbS–organic mesocrystal. Systematic analyses of the orientational relationships between the truncated octahedrally shaped PbS nanoparticles within the *fcc* supperlattice array (models II and III) indicate that the nanoparticles have a tendency toward face-to-face interactions within each closed-packed layer, while keeping a certain degree of orientational mismatch.

In summary, the PbS–organic mesocrystals under investigation were shown to have an intermediate character between high and low orientational ordering of nanoparticles. Furthermore, this system perfectly illustrates the concept of formation and structuring of mesocrystalline materials, which belong to a special class of colloidal crystals.[45,46] The particular case reported herein also represents a missing link on the way to understand general principles governing the formation of PbS–organic colloidal superlattices of nanoparticles with nonspherical (namely truncated octahedrally shaped) inorganic cores. At the same time, this is the first detailed structural characterization of a PbS–organic mesocrystal, which crystallizes in the form of micrometer-sized aggregates with a well-defined faceted habit. The material under investigation is grown by a nonclassical crystallization method and sheds new light on the processes of self-organization and the formation of this fascinating class of mesocrystalline materials.

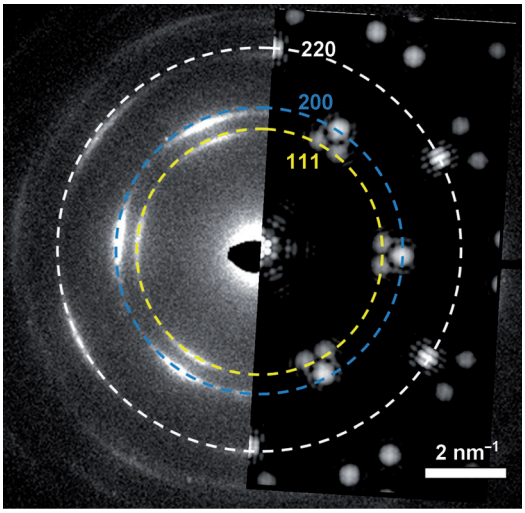

Figure 6. Comparison of the observed (left) and simulated (right) ED patterns detected along $[111]_{SL}$ of the PbS–organic mesocrystal. The simulated ED was obtained by superposition of the ED patterns calculated for the proposed models II and III (see Figure 5). The sets of equidistant (220), (002), and (111) PbS Bragg reflections are marked with white, blue, and yellow circles, respectively.

Experimental Section

Synthesis: In a typical synthesis, lead acetate trihydrate (1.14 g, 3 mmol), oleic acid (3.5 mL, 11 mmol), distilled tri-*n*-octylphosphine (5 mL, 11.2 mmol), and diphenylether (10 mL, 63 mmol) were placed into a three-necked flask, heated under vacuum at 80 °C for 1 h, and subsequently under nitrogen atmosphere to 135 °C for 1 h. After temperature stabilization, a first solution is injected, consisting of thioacetamide (0.08 g, 1.1 mmol), *N*,*N*-dimethylformamide (0.4 mL, 5.1 mmol), and tri-n-octylphosphine (6 mL, 13.5 mmol). After 10 min, a second solution is injected, consisting of thioacetamide (0.02 g, 0.3 mmol), *N*,*N*-dimethylformamide (0.1 mL, 1.3 mmol), and tri-*n*-octylphosphine (0.9 mL, 2 mmol). The reaction mixture is quenched after additional 10 min and the as-synthesized nanoparticles are precipitated and subsequently washed two times with 1-butanol. Afterward, the nanoparticles are redissolved in an organic solvent.

For the formation of colloidal superlattices, a glass tube with a vertically positioned silicon wafer is filled with the solution of the nanoparticle (1 mL). Precipitation is induced by slow percolation of a nonsolvent (methanol or ethanol). The tubes are stored in the dark until precipitation is finished.

Scanning electron microscopy: The morphology and inner structure of the aggregates were studied by scanning electron microscopy (SEM) and transmission electron microscopy (TEM). SEM investigations were performed by means of an ESEM FEI Quanta 200 FEGi system operated in low-vacuum (60 Pa) as well as in high-vacuum mode (2×10^{-4} Pa) at acceleration voltages between 15–25 kV (FEI company, Eindhoven, NL). For investigation under high vacuum, the samples were coated by a thin gold layer (for 30 seconds) in order to obtain a conductive surface. Both, back scattered and secondary electron images were recorded. Figures 1 a,b were recorded using a SEM DSM 982 GEMINI with a field emission gun from Zeiss, Oberkochen, Germany at 3 kV in order to avoid charging.

FIB thin cut preparation: For TEM investigations, focused ion beam (FIB) thin cuts of the aggregates were prepared by means of a FEI Quanta 200 3D dual beam device (FEI company, Eindhoven, NL). For this purpose, selected particles from an ethanol suspension were deposited onto a copper half-ring and the selected region was covered with a protective layer of platinum (thickness 1–2 μm, acceleration voltage 30 kV, current 0.3 nA). After these preparations, the particles were thinned down to electron transparency (thickness of 100–200 nm) by use of the FIB system at 30 kV acceleration voltage. Currents of 3–0.05 nA were used for the Ga^+-beam.

Single-crystal X-ray diffraction: In order to investigate the orientational order of nanoparticles within the complete volume of a colloidal nanocrystal assembly, single-crystal XRD measurements were performed. An octahedrally shaped specimen of the PbS–organic mesocrystal was mounted on a glass capillary. The X-ray diffraction images were collected along [111] of an octahedrally shaped specimen by use of a Rigaku AFC7 & Saturn724+ CCD Detector with Mo-Kα-radiation ($\lambda = 0.71073$ Å).

Transmission electron microscopy: HRTEM experiments on the samples were carried out at the Special Laboratory Triebenberg for Electron Holography and High-Resolution Microscopy at the TU Dresden. A field-emission microscope CM 200 FEG/ST-Lorentz (FEI company, Eindhoven, NL) equipped with a Gatan 1 × 1 k slow-scan CCD camera was used. The analyses of the TEM images were realized by means of the Digital Micrograph software (Gatan, USA). TEM diffraction and middle resolution images were performed by using a FEI Tecnai 10 electron microscope (FEI company, Eindhoven, NL) with a LaB_6 source at 100 kV acceleration voltage and at a camera length of 380 and 750 mm. Images were recorded with a Tietz slow-scan CCD F224HD TVIPS camera (2k × 2k pixels, pixel size 24 μm, digitisation 16 bit) with an active area of 49 mm × 49 mm (Tietz Video and Image Processing Systems GmbH, Gauting, Germany).

Structure modelling: To model the structure of an individual nanoparticle, a cluster with the shape of a truncated octahedron was cut out of the crystal structure of PbS (galena). To this end, atoms within a 8 × 8 × 8 cubic cell ($a = 4.749$ nm) were generated and some of them were removed (according to the algorithm[47]) in order to introduce (111) faces of a nanoparticle (visualisation was performed with the VESTA 3 software[48]). The diameter of such a cluster is around 5.3 nm (estimated as a diameter of the circumscribed sphere), which agrees reasonably well with the experimentally determined size of the nanoparticles (≈ 5.5 nm). These clusters were arranged at the nodes of an *fcc* (super)lattice (with $a = 15.4$ nm), giving rise to an idealised model of a mesocrystal with symmetry $Fm\bar{3}m$ (model I). To take account of different orientations of individual nanoparticles relative to the superlattice, two additional models were constructed: models II and III (for further details see text). The space-group symmetry of each model was checked with the program PLATON.[49] Electron-diffraction patterns were simulated with the program JEMS (version: 3.5930U2010).[50] Cif files of all the models can be obtained from the authors upon request.

Received: June 12, 2012
Published online: September 25, 2012

Keywords: chalcogenides · electron microscopy · nanomaterials · nanoparticles · self-assembly

[1] M. D. Bentzon, J. van Wonterghem, S. Mørup, A. Thölén, C. J. W. Koch, *Philos. Mag. B* **1989**, *60*, 169–178.
[2] C. B. Murray, C. R. Kagan, M. G. Bawendi, *Science* **1995**, *270*, 1335–1338.
[3] T. Vossmeyer, G. Reck, L. Katsikas, E. T. K. Haupt, B. Schulu, H. Weller, *Science* **1995**, *267*, 1476–1479.
[4] S. A. Harfenist, Z. L. Wang, M. M. Alvarez, I. Vezmar, R. L. Whetten, *J. Phys. Chem.* **1996**, *100*, 13904–13910.
[5] R. L. Whetten, M. N. Shafigullin, J. T. Khoury, T. G. Schaaff, I. Vezmar, M. M. Alvarez, A. Wilkinson, *Acc. Chem. Res.* **1999**, *32*, 397–406.
[6] "Transmission Electron Microscopy and Spectroscopy of Nanoparticles": Z. L. Wang, *Characterization of Nanophase Materials* (Ed.: Z. L. Wang), Wiley-VCH, Weinheim, **2000**.
[7] Z. Tang, N. A. Kotov, M. Giersig, *Science* **2002**, *297*, 237–240.
[8] Z. Tang, Z. Zhang, Y. Wang, S. C. Glotzer, N. A. Kotov, *Science* **2006**, *314*, 274–278.
[9] S. Srivastava, A. Santos, K. Critchley, K.-S. Kim, P. Podsiadlo, K. Sun, J. Lee, C. Xu, G. D. Lilly, S. C. Glotzer, N. A. Kotov, *Science* **2010**, *327*, 1355–1359.
[10] E. V. Shevchenko, D. Talapin, A. Kornowski, F. Wiekhorst, J. Kötzler, M. Haase, A. Rogach, H. Weller, *Adv. Mater.* **2002**, *14*, 287–290.
[11] M. Nagel, S. G. Hickey, A. Fromsdorf, A. Kornowski, H. Weller, *Z. Phys. Chem. Int. J. Res. Phys. Chem. & Chem. Phys.* **2007**, *221*, 427–437.
[12] L. R. Meng, W. M. Chen, Y. W. Tan, L. Zou, C. P. Chen, H. P. Zhou, Q. Peng, Y. D. Li, *Nano Res.* **2011**, *4*, 370–375.
[13] S. M. Rupich, E. V. Shevchenko, M. I. Bodnarchuk, B. Lee, D. V. Talapin, *J. Am. Chem. Soc.* **2010**, *132*, 289–296.
[14] P. Podsiadlo, G. Krylova, B. Lee, K. Critchley, D. J. Gosztola, D. V. Talapin, P. D. Ashby, E. V. Shevchenko, *J. Am. Chem. Soc.* **2010**, *132*, 8953–8960.
[15] Y. Wang, Q. Dai, B. Zou, W. W. Yu, B. Liu, G. Zou, *Langmuir* **2010**, *26*, 19129–19135.
[16] Z. Quan, L. Valentin-Bromberg, W. Siu Loc, J. Fang, *Chem. Asian J.* **2011**, *6*, 1126–1136.
[17] A. L. Rogach, D. V. Talapin, E. V. Shevchenko, A. Kornowski, M. Haase, H. Weller, *Adv. Funct. Mater.* **2002**, *12*, 653–666.

[18] E. V. Shevchenko, D. V. Talapin, A. L. Rogach, A. Kornowski, M. Haase, H. Weller, *J. Am. Chem. Soc.* **2002**, *124*, 11480 – 11485.
[19] M. P. Pileni, *J. Phys. Chem. B* **2001**, *105*, 3358 – 3371.
[20] F. Dang, K. Kato, H. Imai, S. Wada, H. Haneda, M. Kuwabara, *Cryst. Growth Des.* **2011**, *11*, 4129 – 4134.
[21] J. Akhtar, M. A. Malik, P. O'Brien, M. Helliwell, *J. Mater. Chem.* **2010**, *20*, 6116 – 6124.
[22] C. Schliehe, B. H. Juarez, M. Pelletier, S. Jander, D. Greshnykh, M. Nagel, A. Meyer, S. Foerster, A. Kornowski, C. Klinke, H. Weller, *Science* **2010**, *329*, 550 – 553.
[23] R. Vogel, P. Hoyer, H. Weller, *J. Phys. Chem.* **1994**, *98*, 3183 – 3188.
[24] S. A. McDonald, G. Konstantatos, S. Zhang, P. W. Cyr, E. J. D. Klem, L. Levina, E. H. Sargent, *Nat. Mater.* **2005**, *4*, 138 – 142.
[25] G. Konstantatos, I. Howard, A. Fischer, S. Hoogland, J. Clifford, E. Klem, L. Levina, E. H. Sargent, *Nature* **2006**, *442*, 180 – 183.
[26] A. L. Rogach, A. Eychmüller, S. G. Hickey, S. V. Kershaw, *Small* **2007**, *3*, 536 – 557.
[27] D. V. Talapin, J.-S. Lee, M. V. Kovalenko, E. V. Shevchenko, *Chem. Rev.* **2010**, *110*, 389 – 458.
[28] B. Lee, P. Podsiadlo, S. Rupich, D. V. Talapin, T. Rajh, E. V. Shevchenko, *J. Am. Chem. Soc.* **2009**, *131*, 16386 – 16388.
[29] Z. Quan, J. Fang, *Nano Today* **2010**, *5*, 390 – 411.
[30] J. J. Choi, C. R. Bealing, K. F. Bian, K. J. Hughes, W. Y. Zhang, D. M. Smilgies, R. G. Hennig, J. R. Engstrom, T. Hanrath, *J. Am. Chem. Soc.* **2011**, *133*, 3131 – 3138.
[31] K. Bian, J. J. Choi, A. Kaushik, P. Clancy, D.-M. Smilgies, T. Hanrath, *ACS Nano* **2011**, *5*, 2815 – 2823.
[32] B. W. Goodfellow, B. A. Korgel, *ACS Nano* **2011**, *5*, 2419 – 2424.
[33] R. Zheng, H. Gu, B. Xu, K. K. Fung, X. Zhang, S. P. Ringer, *Adv. Mater.* **2006**, *18*, 2418 – 2421.
[34] S. C. Glotzer, M. J. Solomon, *Nat. Mater.* **2007**, *6*, 557 – 562.
[35] B. K. Vainshtein, *Fundamentals of Crystals. Symmetry, and Methods of Structural Crystallography*, 2nd ed., Springer, Berlin, **1994**.
[36] B. A. Korgel, S. Fullam, S. Connolly, D. Fitzmaurice, *J. Phys. Chem. B* **1998**, *102*, 8379 – 8388.
[37] U. Agarwal, F. A. Escobedo, *Nat. Mater.* **2011**, *10*, 230 – 235.
[38] An *fcc* arrangement of truncated octahedra can be achieved by continuously increasing the distances between the polyhedra in the Voronoi tiling of the bcc lattice.[39] In other words, an *fcc* arrangement of truncated octahedra can be considered as a "squashed" (in our case by organic macromolecules) Voronoi tiling of the *bcc* lattice.
[39] E. Koch, *Z. Kristallogr.* **1984**, *166*, 23 – 52.
[40] C. A. Rogers, *Packing and Covering*, Cambridge University Press, Cambridge, **1964**.
[41] V. A. Blatov, *Crystallogr. Rev.* **2004**, *10*, 249 – 318.
[42] J. H. Wernick, *Am. Mineral.* **1960**, *45*, 591 – 598.
[43] H. Lichte, P. Formanek, A. Lenk, M. Linck, C. Matzeck, M. Lehmann, P. Simon, *Annu. Rev. Mater. Res.* **2007**, *37*, 539 – 588.
[44] D. V. Talapin, E. V. Shevchenko, C. B. Murray, A. V. Titov, P. Král, *Nano Lett.* **2007**, *7*, 1213 – 1219.
[45] H. Cölfen, M. Antonietti, *Mesocrystals and Nonclassical Crystallization*, Wiley, Chichester, **2008**.
[46] R.-Q. Song, H. Cölfen, *Adv. Mater.* **2010**, *22*, 1301 – 1330.
[47] "Geometric Tools for Computer Graphics": P. J. Schneider, D. H. Eberly, *The Morgan Kaufmann Series in Computer Graphics and Geometric Modeling*, Elsevier, Dordrecht, **2003**, p. 708.
[48] K. Momma, F. Izumi, *J. Appl. Crystallogr.* **2011**, *44*, 1272 – 1276.
[49] A. L. Spek, *Acta Crystallogr. Sect. D* **2009**, *65*, 148 – 155.
[50] P. Stadelmann, Jems, (http://cimewww.epfl.ch/people/stadelmann/jemswebsite/jems.html).

